X-612-65-226

ROCKET MEASUREMENTS OF SQ. CURRENTS AT MID-LATITUDE

BY

T. N. DAVIS

J. D. STOLARIK

J. P. HEPPNER

JUNE 1965

NASA — GODDARD SPACE FLIGHT CENTER

GREENBELT, MARYLAND

Rocket Measurements of Sq Currents at Mid-Latitude

By

T. N. Davis

J. D. Stolarik

J. P. Heppner

June 1965

Rocket Measurements of Sq Currents at Mid-latitude

T. N. Davis, J. D. Stolarik and J. P. Heppner

Abstract

18353

Rubidium-vapor magnetometers were flown to altitudes near 150 km over Wallops Island, Virginia in four Nike-Apache rockets. Two flights were made at times when no ionospheric current was expected and none was encountered. The other two flights measured a current sheet with lower edge at 105 km and upper edge at 123 km, with the total current being in agreement with that expected from the ground observations. One of the flights not encountering measurable ionospheric current was flown in conjunction with another rocket (Smith and Bedinger, 1965) in order to obtain nearly simultaneous measurements of magnetic field, electron density and winds. The ionospheric current calculated using the electron density and wind data was too small to have been observed by the rocket magnetometer.

I Introduction

Ionospheric currents have been detected by rocket-borne magnetometers flown into the equatorial electrojet (Singer et al., 1951; Cahill 1959a), the auroral electrojet (Meredith et al., 1961) and in the northern polar cap (Cahill, 1959b). Similar attempts to detect mid-latitude ionospheric currents have been generally unsuccessful until this year (Burrows and Hall, 1964) because of one or more of the following problems: uncertain knowledge of the reference magnetic field, rocket trajectory errors, low precision of the magnetic field measurement, the low current density in the mid-latitude ionosphere, and the relative insensitivity of total field magnetometers to the magnetic effects of horizontal sheet currents at high magnetic inclination. This paper presents the results of four rocket flights performed at Wallops Island, Virginia (38^{o}N, 75^{o}W) during the period June-October 1964. In this series, double gas cell rubidium-vapor magnetometers were flown in Nike-Apache rockets to altitudes near 150 km.

The change in magnitude of the total magnetic field (ΔF) measured by a magnetometer on its passage through a horizontal current sheet with height-integrated current J per unit width is given exactly by the law of cosines or with negligible error by $4\pi J \cos I \sin\varphi$ where I is the inclination of the main magnetic field and φ is the horizontal angle between the current direction and the direction of H. Due to the $\sin\varphi$ dependence of the measured ΔF, the rocket-borne magnetometer is most sensitive to east-west currents. At the surface of the earth

these produce variations primarily in H, the horizontal intensity, rather than D, the declination, which is sensitive to meridional currents.

A variation in the horizontal component observed at the ground, ΔH_{obs}, consists of a component ΔH_{ex}, due directly to ionospheric current, and a component ΔH_{in}, due to current induced in the earth. Assuming the ratio $\Delta H_{ex}/\Delta H_{in}$ is 1.5, then

$$\Delta H_{obs}(\gamma) = 1.67\Delta H_{ex} = (1.67)(2\pi J) = (1.67)(2\pi)\left(\frac{\Delta F}{4\pi \cos I}\right)$$
$$= 2.44\ \Delta F(\gamma)$$

where J is the height-integrated current per unit width and the inclination I is taken as 70°; ΔF is the change in the scalar field as the rocket magnetometer passes through the current sheet.

II Instrumentation

This study is the first making use of rubidium vapor magnetometers flown in small rockets to study ionospheric currents. In this magnetometer the Zeeman splitting of atomic energy levels in Rb-85 vapor is detected as resonance absorption of light from a Rb-85 source. The frequency of resonance, the Larmor frequency, is a direct measure of the total scalar magnetic field intensity by the relationship

$$f(\text{cps}) = 466744F \pm (K)359\ F^2$$

for a one cell magnetometer where F is in gauss and K, usually < 0.5, indicates the fraction of the constant with F^2 that appears in a given instrument. Here a self-oscillating, cross-coupled, dual cell arrangement is used to largely eliminate the F^2 dependence so that the variation with orientation is small, less than $\pm 2\gamma$ at F= 0.5 gauss. Dual

(or single) cell rubidium magnetometers have null regions (regions of low signal amplitude) of conical shape centered on the instrument optical axis and in the form of a zone centered on the plane perpendicular to the optical axis; the instruments flown in this study have conical nulls of half-angle near 10° and zonal nulls of half-width 5° or less.

In each rocket the magnetometer sensor was mounted in the forward end of the nose cone with the magnetometer optical axis inclined 45° to the rocket axis. In this orientation and with the rocket spin-stabilized at 5-6 rps, null regions were avoided since the magnetic field inclination at Wallops Island, Virginia is 70°.

The Larmor frequency output of each magnetometer was used to phase-modulate a 231.4 Mc, 2-watt telemetry transmitter fed to a 4-element turnstile antenna located at the base of the payload. Other payload components included a battery pack consisting of 20 HR1 silver cells to supply power for the magnetometer and transmitter, a switching module containing partially-shielded relays for switching operations on the ground, and a DOVAP (doppler) transponder for trajectory determination to supplement and check the radar tracking. The DOVAP transponder was connected to 36.8 Mc (input) and 73.6 (output) shroud antennas attached to the Apache rocket motor.

Magnetic materials in the payload components were kept to a minimum and care was used to reduce possible current loops in the payload wiring. The greatest possible separation between the magnetometer

sensor and the other payload components was maintained. The structural parts of the payload and the nose cone were constructed primarily of fiberglass to reduce permanent and induced magnetic fields. As a result, the magnetic contribution of each payload was 2γ or less as measured at the position of the sensor in a zero ambient field.

It is necessary to maintain the magnetometer sensor lamp bulb and absorption cell temperatures within a narrow range for proper operation. The payloads contained circuits allowing measurement and control of the lamp bulb and absorption cell temperatures prior to rocket firing. In flight, the heat output from the lamp together with thermal insulation about the sensor sufficed to maintain operating temperatures within allowable limits.

III Data Recovery and Reduction

On the ground the Larmor-frequency modulated telemetery signal is received and the Larmor-frequency modulation is recorded on magnetic tape together with a reference frequency, time-code and tape recorder speed-lock reference signal. Using a system designed primarily for reduction of satellite data, the rubidium Larmor frequency is counted to an accuracy of one part in 5×10^6. This accuracy is achieved by use of the rubidium signal to gate the interval over which a 5 Mc reference signal is counted. Thus, if a sample period of 0.1 sec is desired, the Larmor frequency can be measured sufficiently accurately to allow a 0.5 gauss magnetic field to be determined with a precision of 0.1 gamma. Once the Rb-85 Larmor frequency is counted, a value of

the scalar magnetic field is found representing the average field over the sampling interval. In a high-speed computer, radar or DOVAP trajectory data are merged with the magnetometer data. At the mid-point of each sampling interval, the location of the rocket is calculated and for that location a reference magnetic field is computed using the coefficients of a spherical harmonic expansion of the geomagnetic field. The computed reference field (B_c) is subtracted from the measured field (B_m); the value of $B_m - B_c$ is then available for printing or automatic plotting versus spatial parameters or time.

IV Presentation of Data

A. Magnetic Conditions

Wallops Islands, Virginia lies to the north of the focus of the equivalent current system derived from the world-wide Sq magnetic variations. The normal variations on undisturbed days is typified by the reproduction of the Fredericksburg magnetogram in Figure 1 (Fredericksburg is 180 km to the west of Wallops Island). The Z component shows minor variation; eastward and westward declinations appear in the morning and afternoon hours, respectively, and the maximum negative H deviation occurs one to two hours before local noon. Thus the maximum change in the total field ΔF measured by a rocket-borne magnetometer on its passage through the ionospheric current sheet is expected just prior to noon when $|-\Delta H|$ is greatest.

One of the flights (F1.14.157) was made on the day represented in Figure 1 during an interval in which no ionospheric current was

expected on the basis of study of the Fredericksburg magnetic recordings obtained on the several days preceding the flight. The H reference line of Figure 1 represents the value of H deduced for the condition of no overhead current. One minute after the commencement of Fl. 14.157, a small pulsation event occurred; its maximum peak-to-peak amplitude was 5γ in H and 2γ in F: see the upper right panel of Figure 1.

Flight 14.156 was launched earlier in the same local day at a time when ΔH at the ground was -44γ: see Figure 1. The period represented by Figure 1 was rather quiet magnetically but was not one of the designated 10 quiet days of June 1964; Kp ranged from 1_o to 2_o and the Fredericksburg K-values were 1 or 2.

A third flight 14.155 was made on June 10, 1964, the most disturbed day in June: see Figure 2. At the time of the flight Kp was 3_o and the Fredericksburg K-value was 2. As in the case of Fl. 14.156, this flight was made during the pre-noon hours when the maximum westward Sq current was expected. Since the flight occurred during a storm period, the horizontal magnetic field was decreased by Dst currents presumed to flow well beyond the ionosphere. Examination of the Fredericksburg magnetograms taken on the days before and after June 10 indicates that the Dst depression of H amounted to approximately 14γ on that day. That determination accounts for the H reference line on Figure 2 being displaced as compared to that on Figure 1. After removal of the Dst depression there remains on Figure 2 a -35γ deviation

in H which one expects to be caused by westward ionospheric currents and related earth-induced currents.

A fourth flight (Fl. 14.159) was launched on October 8, 1964 in conjunction with a sodium-release rocket flight during morning twilight. The Fredericksburg magnetogram covering the period of this flight is reproduced in Figure 3. Although this was not one of the designated quiet days in October, 1964 the level of magnetic activity was not high during the first half of October 8: Kp ranged from 2_o to 3_o and the K-value at Fredericksburg was 2 or 3. At the time of Fl. 14.159, the Fredericksburg H-component trace was within 3γ of its quiet-day level so the flight was not expected to encounter ionospheric current.

In summary, Fls. 14.157 and 14.159 occurred at times of minimal ΔH and were not expected to detect sizable ionospheric current. Flights 14.155 and 14.156 occurred when ΔH was $-33 \pm 7\gamma$ and $-42.5 \pm 2.5\gamma$, respectively; hence these flights should have encountered detectable ionospheric current.

The horizontal paths of the four rocket flights are indicated on a map (Figure 4) showing the magnitude of the total magnetic field at the earth surface as computed from the coefficients of the spherical harmonic expansion of the geomagnetic field given by Leaton and Evans (1964). Actual departures from the computed surface field are indicated in the form of contours drawn at 100γ intervals. Although the anomaly contours drawn in the upper-left corner of Figure 4 are based on recent

comprehensive data, the anomaly values elsewhere on Figure 4 are derived from very few data points obtained over the past 15 years. Consequently, only the gross features of the anomaly map should be considered as meaningful.

The significant features of Figure 4 for our purpose are a generally increasing anomaly field from the launch point (upper left) to the rocket impact points and an isolated region of higher field near the impact point of Fl. 14.156. Relative to the magnetic field computed from the Leaton and Evans coefficients, the rocket magnetometers should measure higher fields near the impact points than measured near the launch point. Flight 14.159 is somewhat of an exception in that its impact point is beyond the main anomalous region.

B. Flight Data

The flight data were sampled over a period equal to the appropriate rocket roll period (0.17 to 0.25 sec). By sampling at this rate, errors which are dependent upon the angular orientation of the rocket measured in the plane perpendicular to its spin axis are averaged out. The result is a measurement of the scalar field independent of the spin and which is precise to within a fraction of one gamma. This measurement gives the magnitude of the vector sum of the local geomagnetic field and the spin-axis component of the rocket's magnetic field. Flight data above altitude 70 km from the ascent portions of all flights are shown in Figure 5.

The data points on Figure 5 exhibit a sinusoidal variation indicating a magnetic contribution along the spin-axis of each rocket

and a precessional motion of the rocket with a period near 30 seconds. Although each payload is known to possess a very minor magnetic field ($\leq 2\gamma$), the overall vehicle (payload and attached Apache stage) showed a magnetic field component along the spin axis of 30 to 50γ, as measured during re-entry turn-over. This field was due to magnetic elements within the rocket motor or to currents induced by the high spin rates. Due to the smoothness in the variation of the precession period and angle during the upper portion of each flight, it is possible to apply a precession correction to the data of the form $C \sin \omega t$. The results of such point by point corrections are indicated in Figure 5 by the solid lines drawn through the data points. The shaded regions enclosing the curves for Fls. 14.155 and 14.156 represent a generous estimate of the uncertainty in the precession correction; very little uncertainty exists in the correction applied to Fls. 14.157 and 14.159. All flight data taken in the region above 80 km is shown in Figure 6 with precession corrections applied.

Before considering in detail the flight data obtained above 80 km, we draw attention to the overall flight data, especially the part taken at low altitude where the effects of ground anomalies are most important. Plots of all flight data are given in Figures 7-10. As seen in these diagrams, near the beginning of each flight the flight magnetometer measured a field of 100 or more gammas less than that calculated from the Leaton and Evans reference field. This difference is in accord with that expected from examination of the anomaly map,

Figure 4. The ascent portion of each flight shows a steadily increasing value of B_m-B_c with altitude; the rate of increase lessens with altitude to the 90 km level. The lessening rate of increase with altitude evidently reflects the fall-off with distance of the ground anomaly field. Except for Fl. 14.159 (Figure 8), the anomaly field appears to have little effect on the ascent data taken above 100 km. As seen in Figure 4, the descent portions of each flight occur over the region of highest surface anomaly field; this is reflected in the measurements at high altitude by the descent B_m-B_c values generally being higher than those measured during ascent: see Figures 7-10.

Below the 100 km level, the descent portions of Fls. 14.155, 14.156 and 14.157 show monotonically increasing B_m-B_c values to rocket impact, at which points the measured fields were 200γ or more above the Leaton and Evans reference field values. Flight 14.159 passed over the main anomalous region to impact at a point of near-zero surface anomaly and at that point measured a field nearly equal to the reference field value.

Flights 14.157 and 14.159 occurred under identical magnetic conditions and along almost identical flight azimuths. The main difference between the flights was the higher apogee and shorter horizontal range of Fl. 14.157 as compared to Fl. 14.159. The characteristics of the high altitude data from these two flights (see Figure 6) are very similar. In neither case is there any discontinuity in the region above 80 km that

can be attributed to the effect of a current layer in the ionosphere; nor was any expected on the basis of magnetic measurements made on the ground during these flights. In Figure 6, a small change in slope appears near 115 km in the descent portion of the data from Fl. 14.159, but this is the altitude at which the rocket passed over the greatest anomaly measured on its sub-trajectory path. It is not clear whether or not the 14.157 flight magnetometer detected the small pulsation event occurring during the flight but the flight data, especially that taken during the rocket ascent, do indicate that the amplitude of the event could not have been much if any greater at altitude than that observed on the ground.

The ascent data from Fl. 14.155 presented in one panel of Figure 5 shows an increase in $B_m - B_c$ of approximately 11γ between the altitudes 105 and 123 km, which indicates the existence of westward current in this height region. The Fl. 14.155 descent data plot, Figure 6, shows a sharp discontinuity at 105 km and possibly one near 125 km, but evidently the effects of the ionospheric current layer are partially masked by the ground anomaly field. For this flight, a deviation of approximately 14γ in $|F|$ was predicted from the ground observations on the assumption that 0.6 of the observed ΔH was due to external currents. Similarly, a deviation in $|F|$ of 17γ was predicted for Fl. 14.156. Both the ascent and descent plots, Figures 5 and 6, from this flight show discontinuities at 105 and 123 km. The field change in the upward passage through the current sheet was approximately

17γ and the apparent descent field change was near 12γ. However as in the case of Fl. 14.155, the descent data appear to reflect variations caused both by the ionospheric current and by the ground anomaly.

C. Reference Magnetic Fields

Several reference geomagnetic fields (B_c) have been used to make plots of altitude versus B_m-B_c. We find that the slopes and absolute values of the altitude versus B_m-B_c curves differs from one reference field to another (see Fig. 11) but that no essential difference in data interpretation results. Since the Leaton and Evans field results in near-zero B_m-B_c values above altitude 100 km and a more nearly vertical trend in the data plots, this reference field is chosen here.

V Near-Simultaneous Measurement of Electron Density, Wind and Magnetic Field In the Ionosphere

Eleven minutes prior to the October 8, 1964 flight of Fl. 14.159, Smith and Bedinger (1965) launched a rocket in morning twilight for the measurement of electron density and high-altitude wind along a trajectory similar to that of Fl. 14.159. Their rocket carried a Langmuir probe for the measurement of electron density and released an alkali vapor trail for the measurement of horizontal wind direction and speed. The wind measurement results are given in Figure 12 and the results of the electron density measurement appear in Figure 13 together with model electron-neutral collision frequencies computed by Brown (1962).

Using the data given in Figures 11 and 12 and the equations given in Table I the horizontal current is calculated as a function of height; in making this calculation polarization electric fields are ignored. The resulting north-south and east-west current densities are shown in Figure 14. Integration of the current over the height range 80 to 150 Km results in a net northward current of 0.3 amperes/Km and a net westward current of 0.1 amperes/Km. Only the east-west current component contributes to ΔF, the field change measured by a total field magnetometer on its passage through the current sheet. The ΔF resulting from the east-west current also is plotted on Figure 14. This ΔF is too small to have been observed by the Fl. 14.159 magnetometer; even the "discontinuity" at the base of the current sheet is less than $1/3\gamma$. The Fl. 14.159 magnetometer did not detect an ionospheric current, therefore the results of that flight are in agreement with the results of this calculation.

In order to explain the observed magnitude of the noontime Sq depression of H a net westward ionospheric current near 40 amperes/Km is required. If the noontime Sq currents are largely confined to the height range indicated by our flights 14.155 and 14.156 (105-123 Km), then the westward current density in this height range must be 40 to 200 times that calculated for the morning twilight period of October 8, 1964. It must be emphasized that the current density calculation given here is only a partial analysis since polarization effects have been ignored. An appropriate polarization field will increase the

effective current and is likely to be necessary to explain the magnitude of the noontime Sq maximum, only a part of which appears to be accounted for by the normal daytime increase in electron density. At times such as the morning twilight of October 8, 1964, when the ionospheric wind direction markedly varies with height, polarization fields may be unimportant as a consequence of both mutual cancellation and the σ_0 discharge of opposing polarizations along magnetic field lines. It seems likely that the observed noontime Sq current requires a more uniform wind than is observed at twilight and the build-up of an appropriate polarization field to enhance the effective conductivity. Clearly, a method of measuring winds in the ionosphere during the daylight hours is needed.

VI Summary and Discussion

A summary of the results of the four flights together with an estimate of the probable errors is given in Table II. An internally consistent interpretation of the flight data requires magnetic contributions from both ionospheric current and ground anomalies. The ground anomaly contribution to the ascent data is minor and poses no interpretative problem. However, the descent portions of all flights pass over an appreciable anomaly which has sufficient magnetic contribution at altitude to prevent a quantitative determination of the ionospheric current contribution from the descent data alone. Since the anomaly magnetic field adds vectorially to the geomagnetic field, a quantitative treatment of its effect on the flight data requires more complete knowledge of the surface anomaly field than is available

from the sparse observations now in hand.

The data from the two flights (Fls. 14.155 and 14.156) which penetrated a detectable current layer indicate a simple westward current sheet lying between altitudes 105 and 123 km with the altitude of maximum current density between 110 and 116 km. The total current within the sheet is in good agreement with that expected from the ground measurements.

Acknowledgments

We are grateful to Mr. J. C. Seddon for his efforts in providing final trajectories from the DOVAP data. Mr. G. F. Hinton, United States Navy Oceanographic Office, provided total field magnetic data from a helium magnetometer operated at Wallops, Island, Virginia.

Figure Titles

Figure No.	Title
1	Tracings of the Fredericksburg magnetogram for June 25, 1964 showing the times of flights 14.156 and 14.157. Panel inserts indicate the detailed magnetic variations during each flight: ΔH from the Fredericksburg rapid-run recording; ΔF from a helium magnetometer operated at Wallops Island. Date is given for left-hand portion of the diagram.
2	Tracings of the Fredericksburg magnetogram for June 10, 1964 with a panel insert showing the detailed magnetic variations during flight 14.155. See also the title for Figure 1.
3	Tracings of the Fredericksburg magnetogram for October 7, 1964 with a panel insert showing the detailed magnetic variations during flight 14.159. See also the title for Figure 1.
4	Map showing the horizontal projections of the rocket flights. The parallel lines running from lower left to upper right represent the Leaton and Evans Epoch 1965 reference field at the earth's surface and the curved contours represent the surface anomaly field referenced to the Leaton and Evans field. Latitudes and longitudes are north and west, respectively.

Figure No.	Title
5	Plots of altitude versus the measured total field minus the computed total field for the ascent portions of all flights; data points taken at intervals of approximately one second. Solid lines represent the data corrected for effects due to vehicle precession.
6	Precession-corrected ascent (open-circle) and descent (full-circle) data taken at intervals of approximately one second above altitude 80 km for all flights.
7	Smoothed data from Fl. 14.157 referenced to the Leaton and Evans field. Effects due to vehicle precession and turn over on re-entry have been removed.
8	Smoothed data from Fl. 14.159; see Figure 7 title.
9	Smoothed data from Fl. 14.155; see Figure 7 title.
10	Smoothed data from Fl. 14.156; see Figure 7 title.
11	Plots of altitude vs. $B_m - B_c$ for Fl. 14.157 using several reference fields given by Cain et al. (1965). Except for the field labeled Jensen - Cain 1960, time-dependent terms are included to compute the reference fields. Note the different $B_m - B_c$ scales.
12	Measurements of wind speed and direction obtained by Smith and Bedinger (1965) from their Fl. 14.194 flown at 1023 u.t. on October 8, 1964 from Wallops Island, Virginia.

Figure No.	Title
13	Electron density measured by Smith and Bedinger (1965) from their Fl. 14.194 flown at 1023 u.t. on October 8, 1964 from Wallops Island, Virginia and nighttime electron-neutral collision frequency computed by Brown (1962).
14	Calculated current densities at the time of Fl. 14.159 (10^h on October 8, 1964) and the resulting change in scalar magnetic field (ΔF) referenced to the bottom edge of the current layer.

BLANK PAGE

References

Brown, L. W., Ionospheric absorption of extraterrestrial radio waves, NASA Rept. I-615-62-194 Goddard Space Flight Center, Greenbelt, Md., 65 pp., October 1962.

Burrows, K., and S. H. Hall, The in situ detection of an ionospheric electric current, Nature, 204, 721-722, 1964.

Cahill, L. H., Investigation of the equatorial electrojet by rocket magnetometer, JGR, 64, 489-503, 1959a.

Cahill, L. J., Detection of an electrical current in the ionosphere above Greenland, JGR, 64, 1377-1380, 1959b.

Cain, J. C., S. Hendricks, W. E. Daniels, and D. C. Jensen, Computation of the main geomagnetic field from spherical harmonic expansions, NASA Rept, X-611-64-316, Goddard Space Flight Center, Greenbelt, Md., 13 pp., October 1964.

Chapman, S., The electrical conductivity of the ionosphere: a review, Nuovo Cimento, 4, 1385-1412, 1956.

Leaton, B. R., and M. J. Evans, An analytical representation of the estimated geomagnetic field and its secular change for the Epoch 1965.0, presented at Symposium on Magnetism of the Earth's Interior, Pittsburgh, Nov. 1964. (See also Cain, J. C., S. Hendricks, W. E. Daniels, and D. C. Jensen, Computation of the main geomagnetic field from spherical harmonic expansions, NASA Rept. X-611-64-316, Goddard Space Flight Center, Greenbelt, Md., 1964.)

Meredith, L. H., L. R. Davis, J. P. Heppner, and O. E. Berg, Rocket auroral investigations, Annals of the IGY, 12, 631, 1961.

Singer, S. F., E. Maple, and W. A. Bowen, Evidence for ionospheric currents from rocket experiments near the geomagnetic equator, JGR, 56, 265-281, 1951.

Smith, L. G., and J. F. Bedinger, Measurement of upper atmospheric ionization and winds with a combined payload, First Quart. Progress Rept., 24 July 1964-31 October, 1964, Geophysis Corp. of America, Bedford, Mass., 15 pp., 1965.

TABLE TITLE

BLANK PAGE

TABLE I

Assumptions:

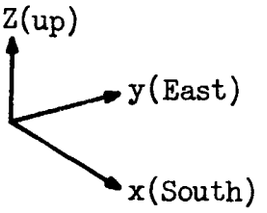

$$E_x = -V_y \left|Z\right| \quad , \quad E_y = V_x \left|Z\right|$$

$$n_i = n_e$$

$$\nu_{i(h)} = \nu_{e(h)}/20 \quad \text{(Chapman, 1956)}$$

Conductivity

$$\sigma_o = e^2 n_e \left(\frac{1}{m_e \nu_e} + \frac{1}{m_i \nu_i} \right),$$

$$\sigma_1 = e^2 n_e \left(\frac{\nu_e}{m_e(\nu_e^2+\omega_e^2} + \frac{\nu_i}{m_i(\nu_i^2+\omega_i^2)} \right)$$

$$\sigma_2 = \frac{-en_e}{F} \left(\frac{\omega_e^2}{\nu_e^2+\omega_e^2} - \frac{\omega_i^2}{\nu_i^2+\omega_i^2} \right)$$

$$\sigma_3 = \sigma_1 + \frac{\sigma_2^2}{\sigma_1}$$

F, Z = total and vertical magnetic field, $\omega_{e,i} = \frac{eF}{M_{e,i}}$

$\sigma_{xx} = \sigma_o \sigma_1/A, \qquad A = \sigma_o \cos^2 70^\circ + \sigma_1 \sin^2 70^\circ$

$\sigma_{xy} = \sigma_o \sigma_2 \sin 70^\circ/A,$

$\sigma_{yy} = \sigma_1(\sigma_o \sin^2 70^\circ + \sigma_3 \cos^2 70^\circ)/A$

Current Density

$J_x = \sigma_{xx} E_x + \sigma_{xy} E_y$ (abamperes/cm^2)

$J_y = -\sigma_{xy} E_x + \sigma_{yy} E_y$ (abamperes/cm^2)

TABLE II

SUMMARY WITH ESTIMATE OF PROBABLE ERRORS

	Flight 14.157 $00^h\ 52^h\ 30^s$ U.T. 26 June 1964	Flight 14.159 $10^h\ 34^m\ 00^s$ U.T. 8 October 1964	Flight 14.155 $15^h\ 10^m\ 00^s$ U.T. 10 June 1964	Flight 14.156 $14^h\ 57^m\ 39^s$ U.T. 25 June 1964
Observed ΔH At Ground	$+3.7 \pm 2.5\gamma$	$-3.0\gamma \pm 2.5\gamma$	$-33.0 \pm 7\gamma$	$-42.5 \pm 2.5\gamma$
Predicted ΔF from Ground Observations Assuming $f = \frac{\Delta H_{ex}}{\Delta H_{obs}} = 0.6$	$+1.5 \pm 1\gamma$	$-1.2 \pm 1\gamma$	$-13.5 \pm 3\gamma$	$-17.5\gamma \pm 1\gamma$
ΔF Observed in Flight	Ascent: $0 \pm 1\gamma$ Descent: $0 \pm 2\gamma$	Ascent: $0 \pm 2\gamma$ Descent: $0 \pm 2\gamma$	Ascent: $-11 \pm 2\gamma$ Descent: ?	Ascent: $-17 \pm 2\gamma$ Descent: $-12 \pm 2\gamma$(?)
Altitude of Lower Edge of Current Sheet	-	-	Ascent: 105 ± 1km Descent: 104 ± 1km	Ascent: 106 ± 1km Descent: 105 ± 1km
Altitude of Maximum Current Density	-	-	Ascent: ~116km(?) Descent: (?)	Ascent: ~110km(?) Descent: ~113km(?)
Altitude of Upper Edge of Current Sheet	-	-	Ascent: 123 ± 1km Descent: (?)	Ascent: 123 ± 1km Descent: 123 ± 1km
Total Westward Horizontal Current	-	-	Ascent: 25.6 ± 1.5 Amperes/km Descent: (?)	Ascent: 39.4 ± 1.5 Amperes/km Descent: > 26 Amperes/km

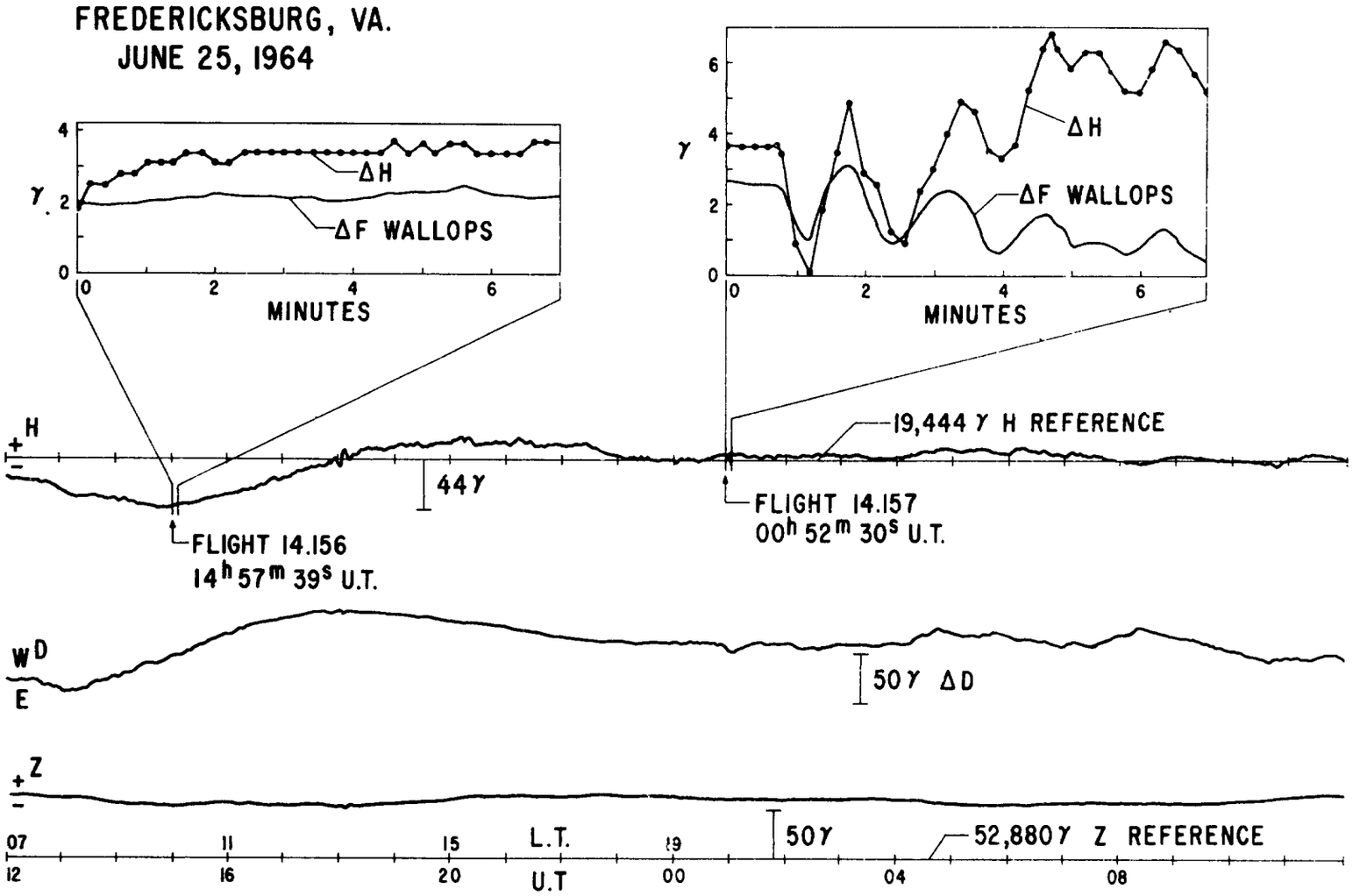

Figure 1 Tracings of the Fredericksburg magnetogram for June 25, 1964 showing the times of flights 14.156 and 14.157. Panel inserts indicate the detailed magnetic variations during each flight: ΔH from the Fredericksburg rapid-run recording; ΔF from a helium magnetometer operated at Wallops Island. Date is given for left-hand portion of the diagram.

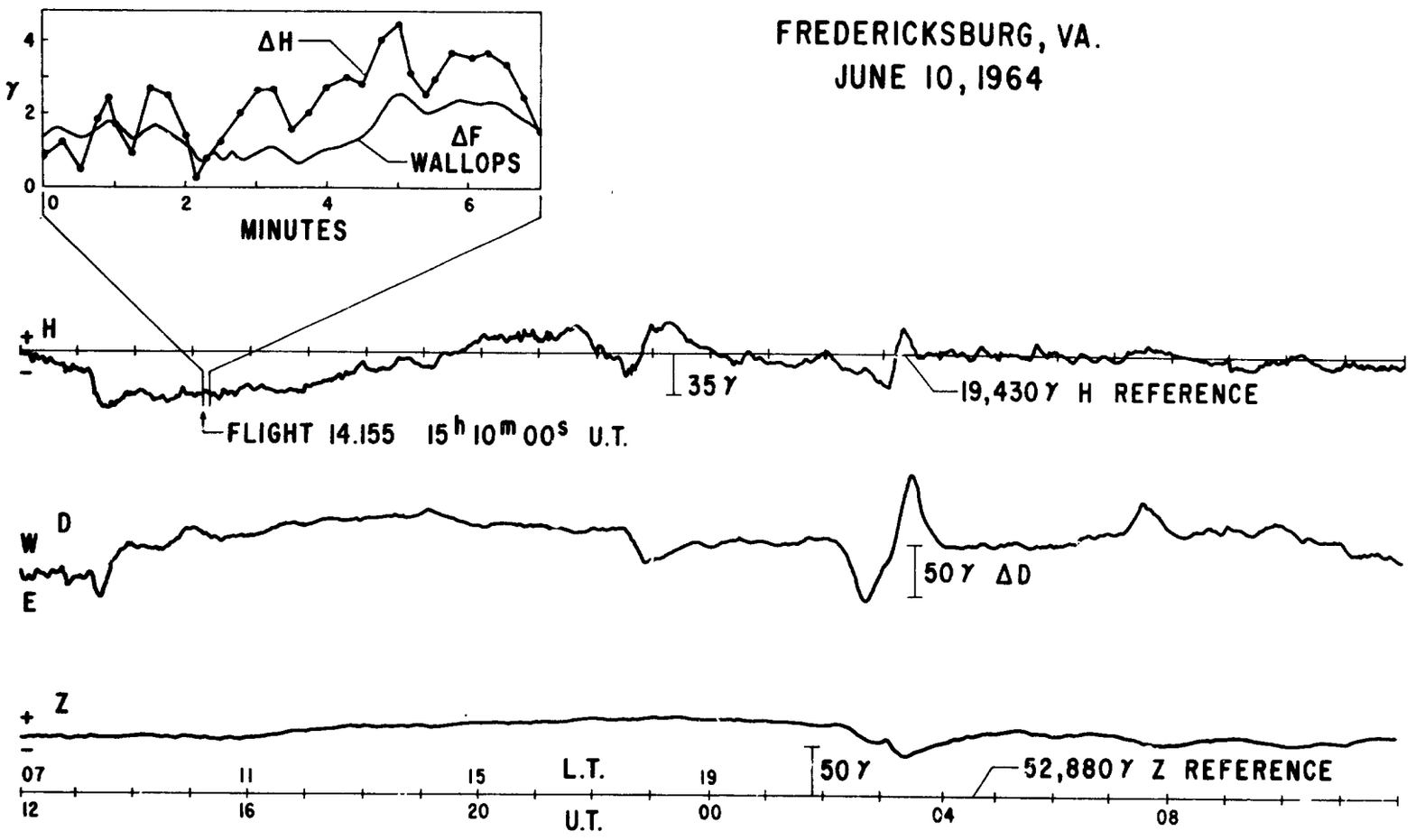

Figure 2 Tracings of the Fredericksburg magnetogram for June 10, 1964 with a panel insert showing the detailed magnetic variations during flight 14.155. See also the title for Figure 1.

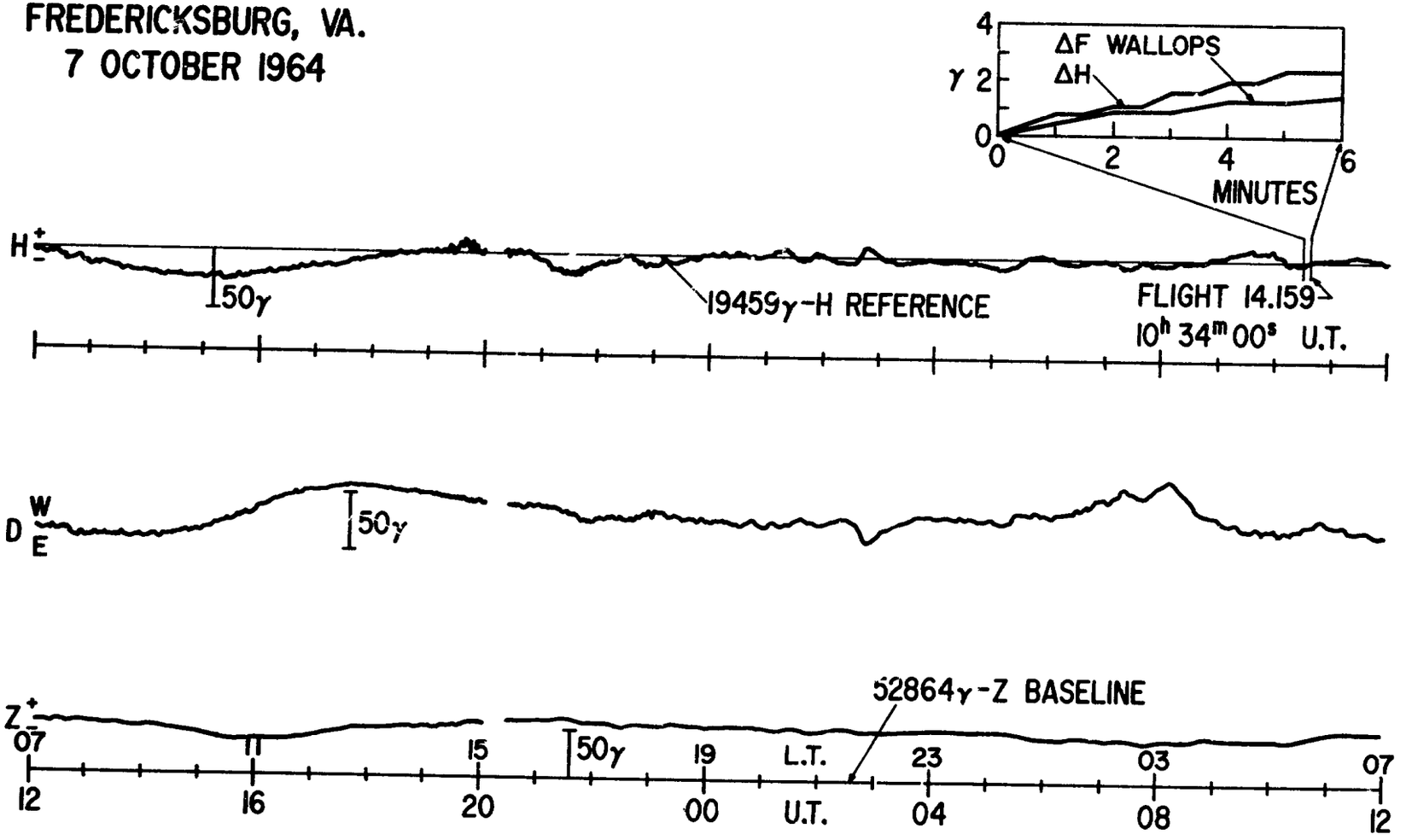

Figure 3 Tracings of the Fredericksburg magnetogram for October 7, 1964 with a panel insert showing the detailed magnetic variations during flight 14.159. See also the title for Figure 1.

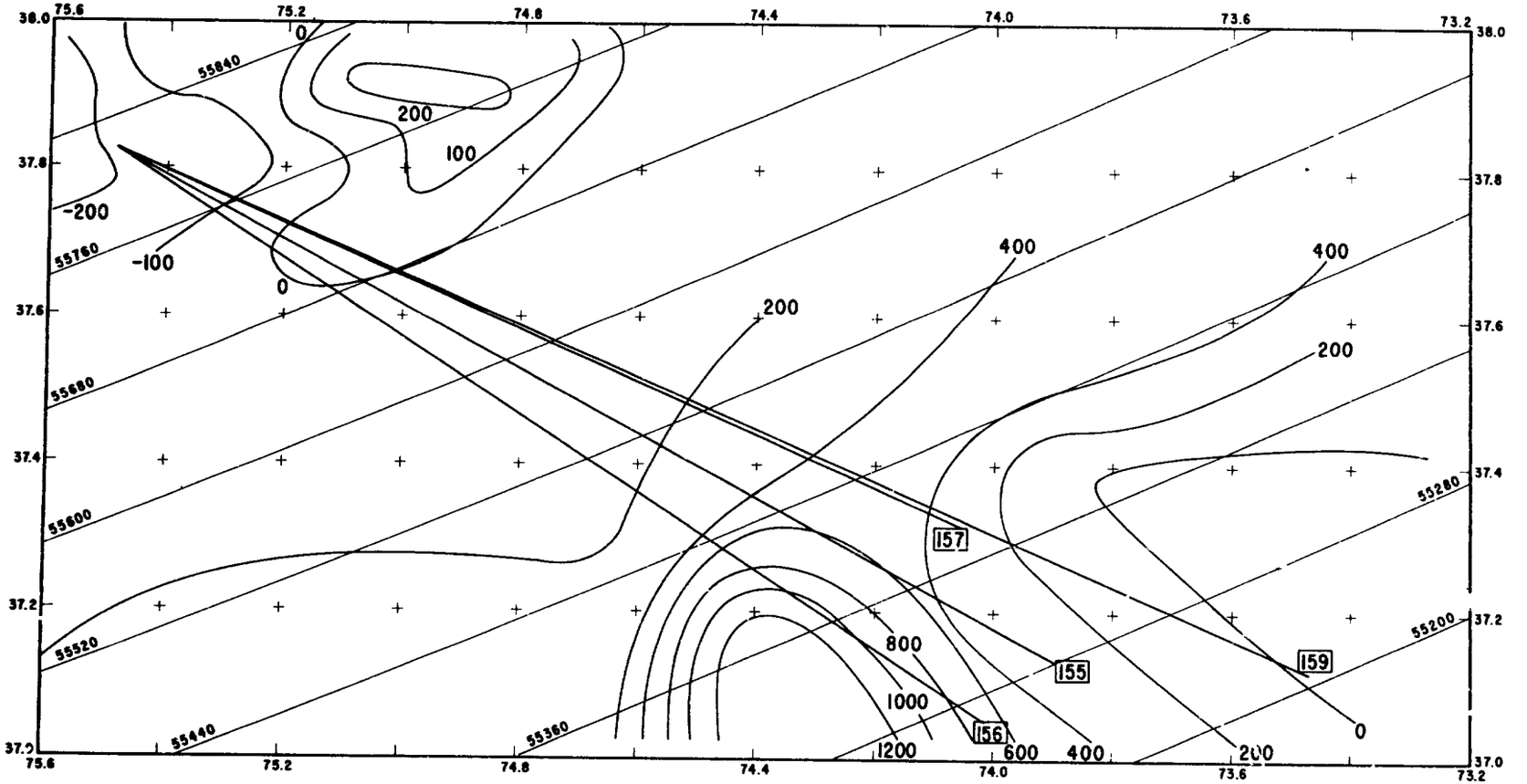

Figure 4 Map showing the horizontal projections of the rocket flights. The parallel lines running from lower left to upper right represent the Leaton and Evans Epoch 1965 reference field at the earth's surface and the curved contours represent the surface anomaly field referenced to the Leaton and Evans field. Latitudes and longitudes are north and west, respectively.

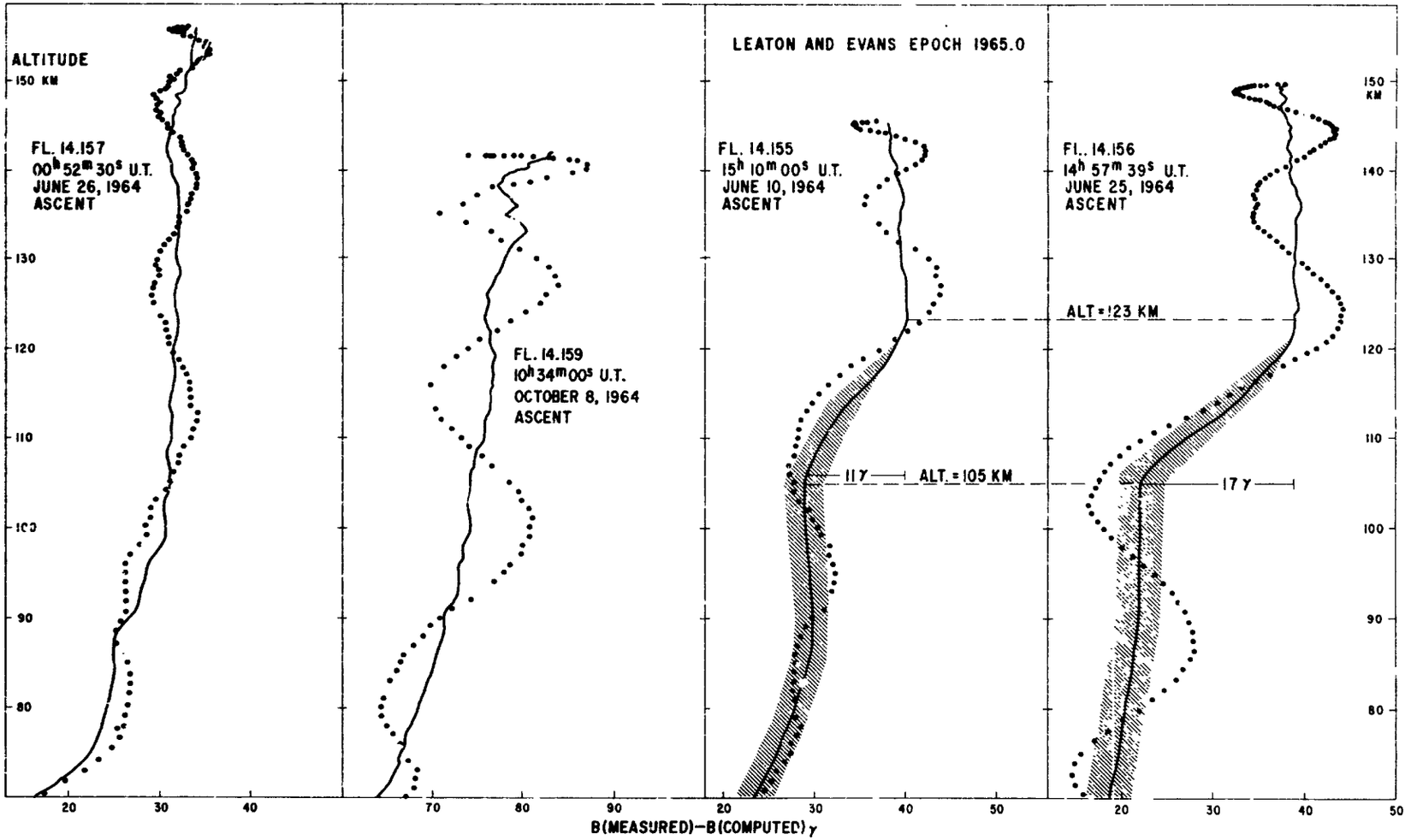

Figure 5 Plots of altitude versus the measured total field minus the computed total field for the ascent portions of all flights; data points taken at intervals of approximately one second. Solid lines represent the data corrected for effects due to vehicle precession.

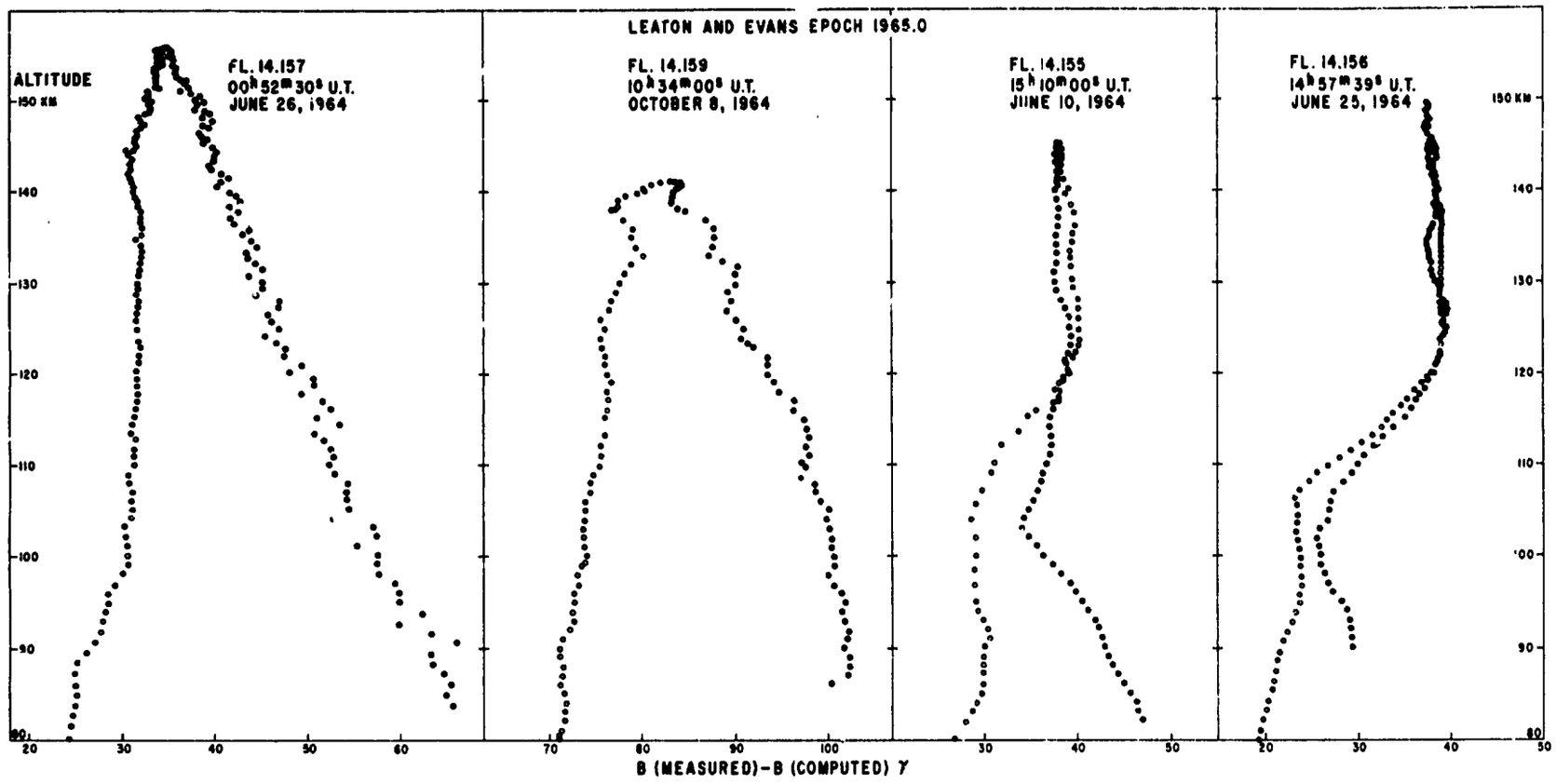

Figure 6 Precession-corrected ascent (open-circle) and descent (full-circle) data taken at intervals of approximately one second above altitude 80 km for all flights.

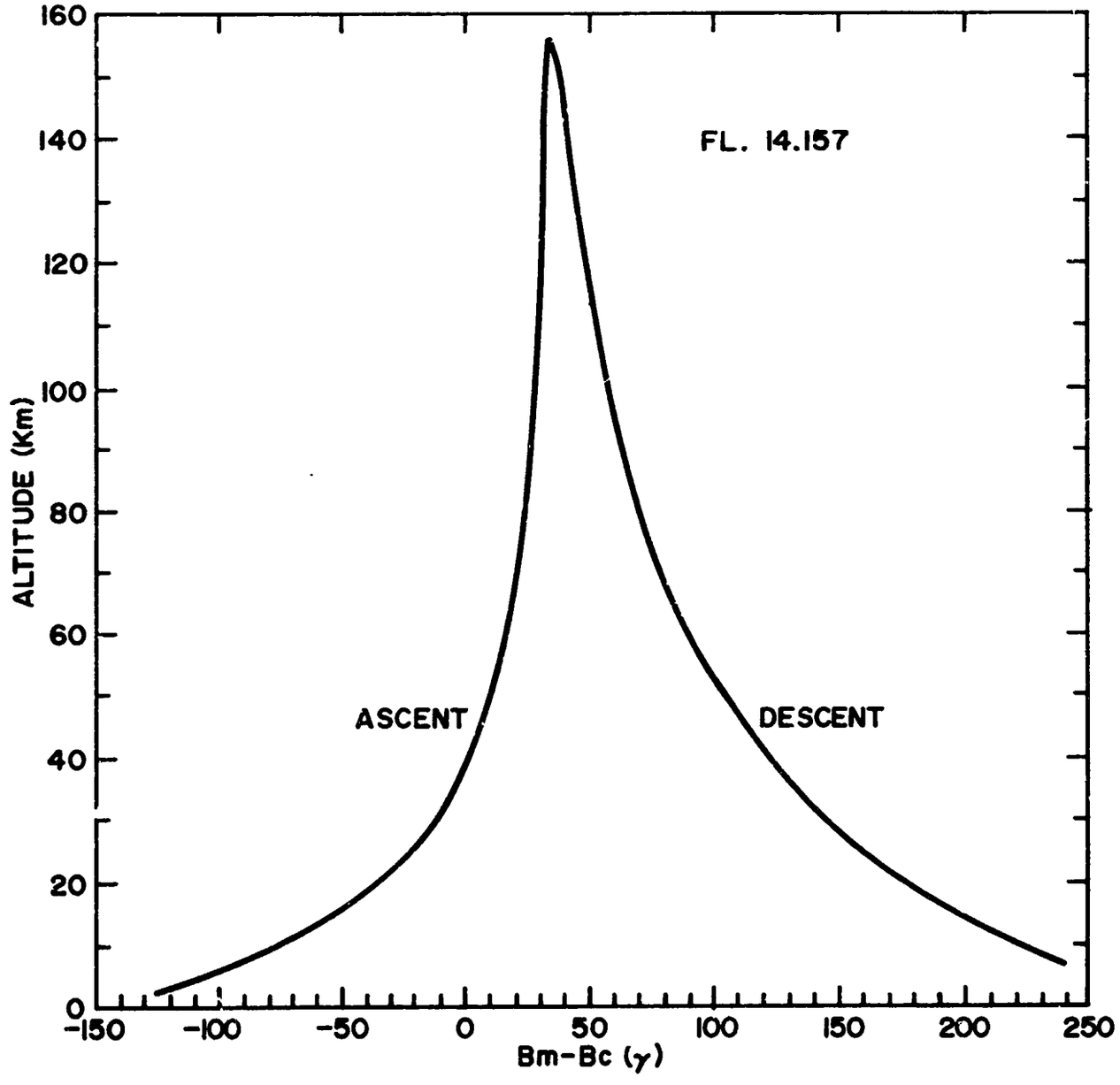

Figure 7 Smoothed data from Fl.14.157 referenced to the Leaton and Evans field. Effects due to vehicle precession and turn over on re-entry have been removed.

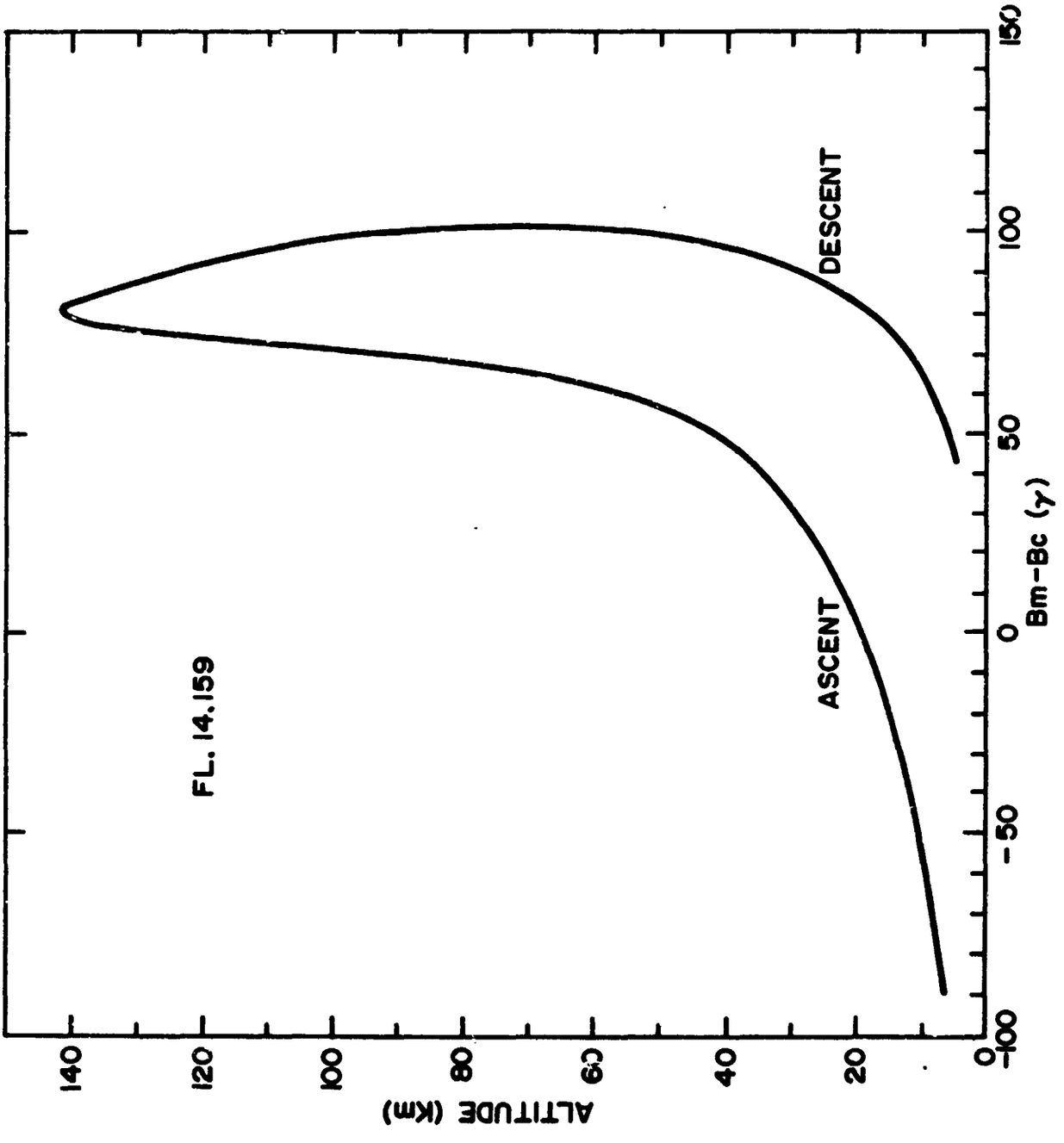

Figure 8 Smoothed data from Fl. 14.159; see Figure 7 title.

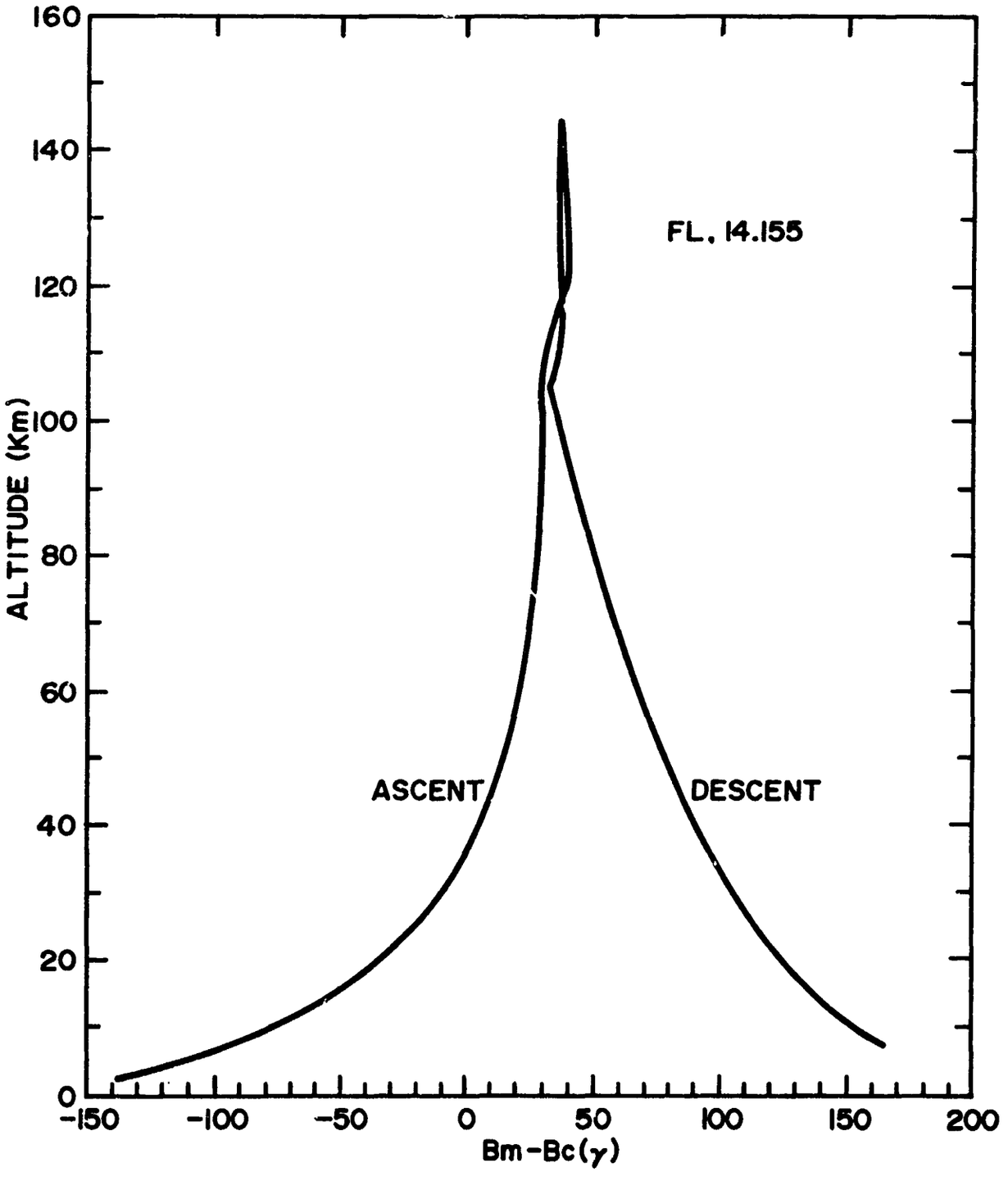

Figure 9 Smoothed data from Fl. 14.155; see Figure 7 title.

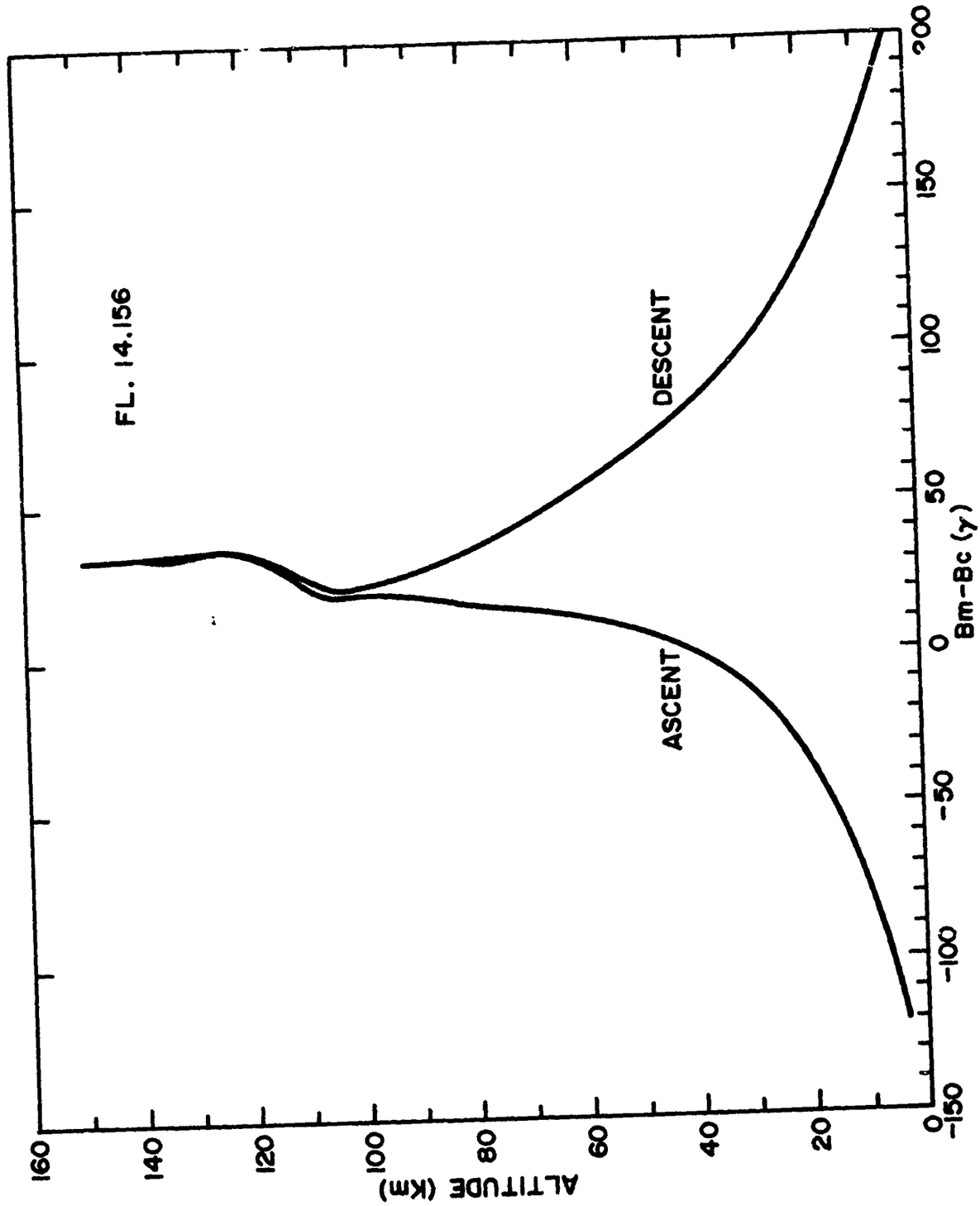

Figure 10 Smoothed data from Fl. 14.156; see Figure 7 title.

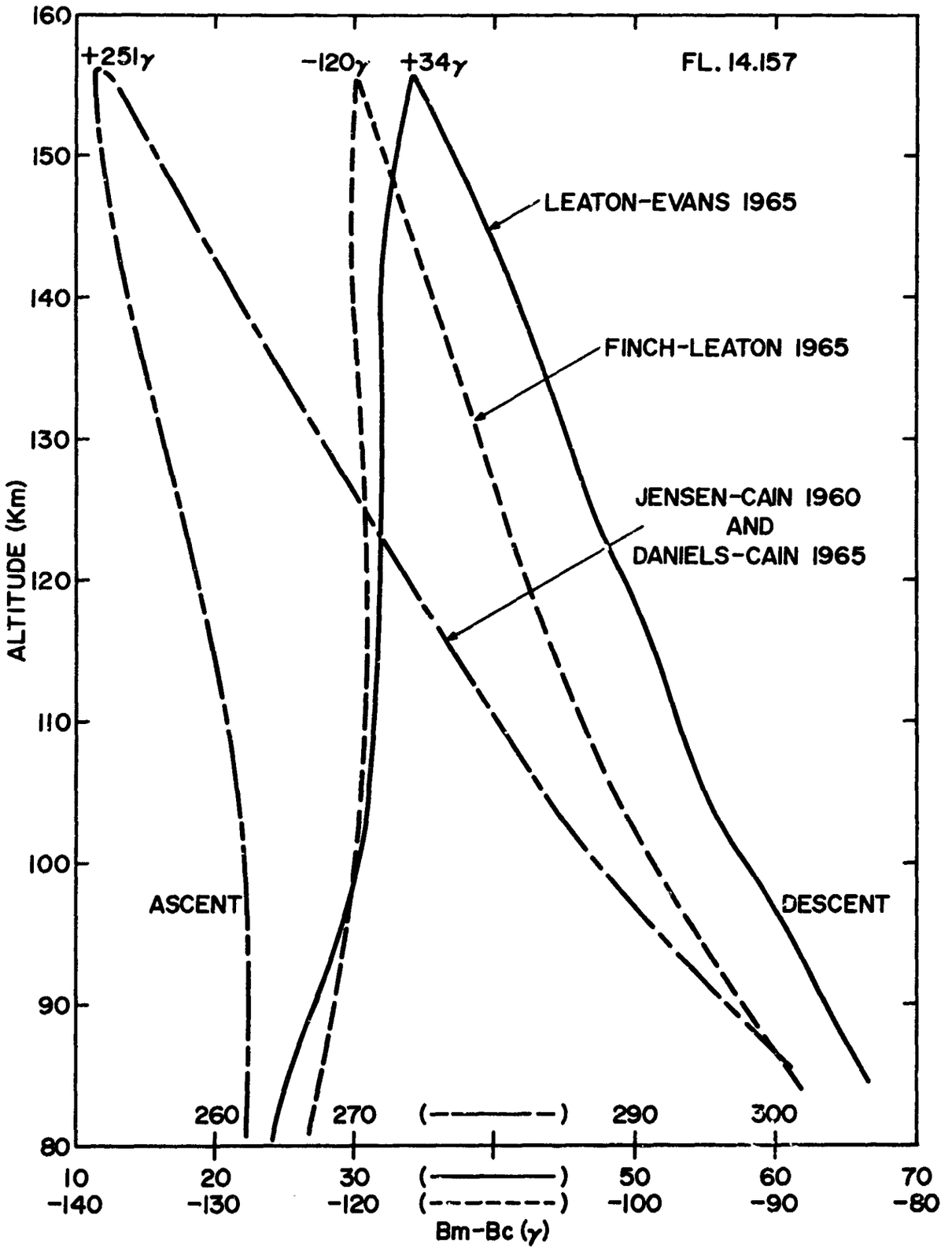

Figure 11 Plots of altitude vs. $B_m - B_c$ for Fl. 14.157 using several reference fields given by Cain et al. (1965). Except for the field labeled Jensen - Cain 1960, time-dependent terms are included to compute the reference fields. Note the different $B_m - B_c$ scales.

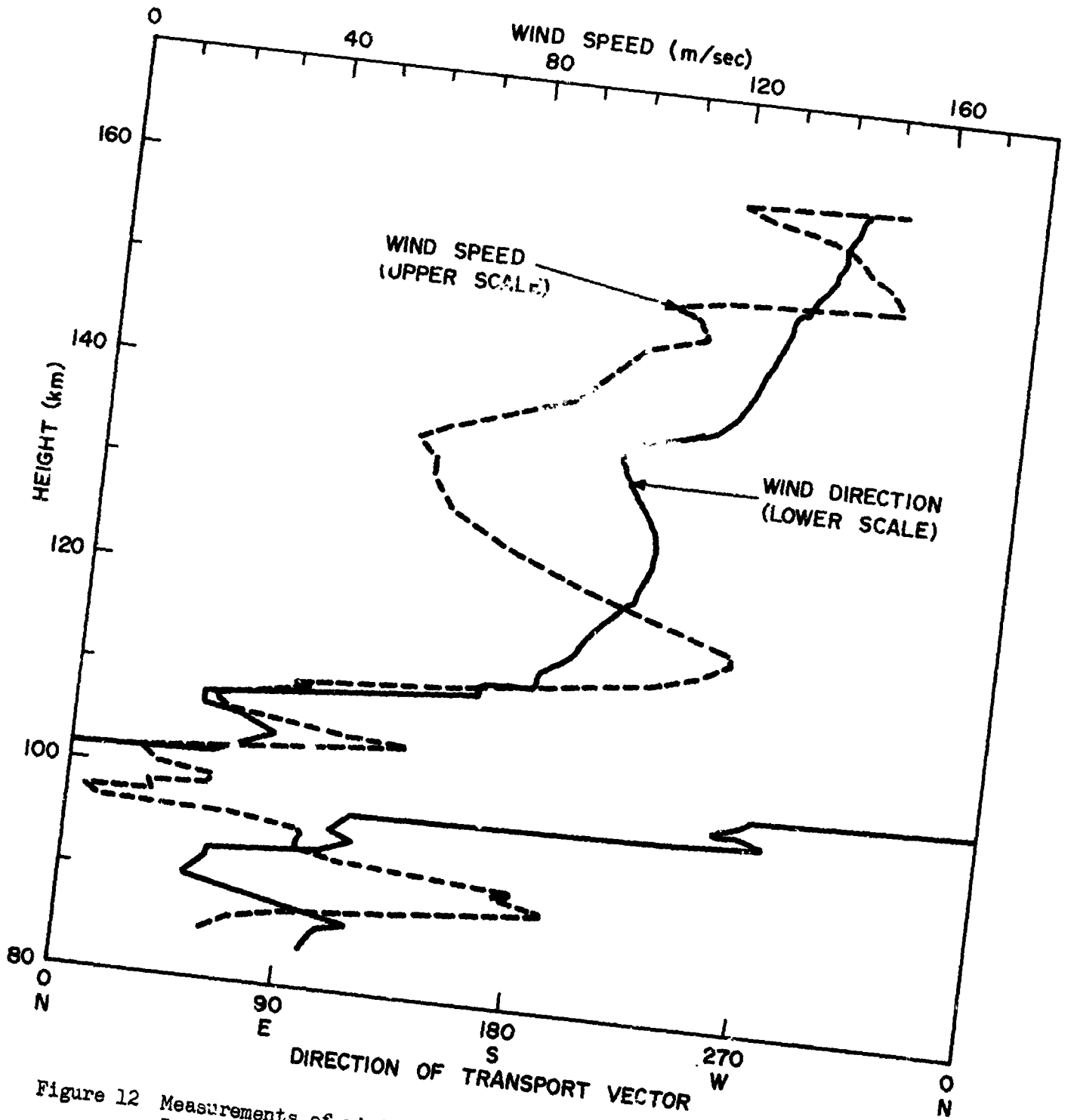

Figure 12 Measurements of wind speed and direction obtained by Smith and Bedinger (1965) from their Fl. 14.194 flown at 1023 u.t. on October 5, 1964 from Wallops Island, Virginia.

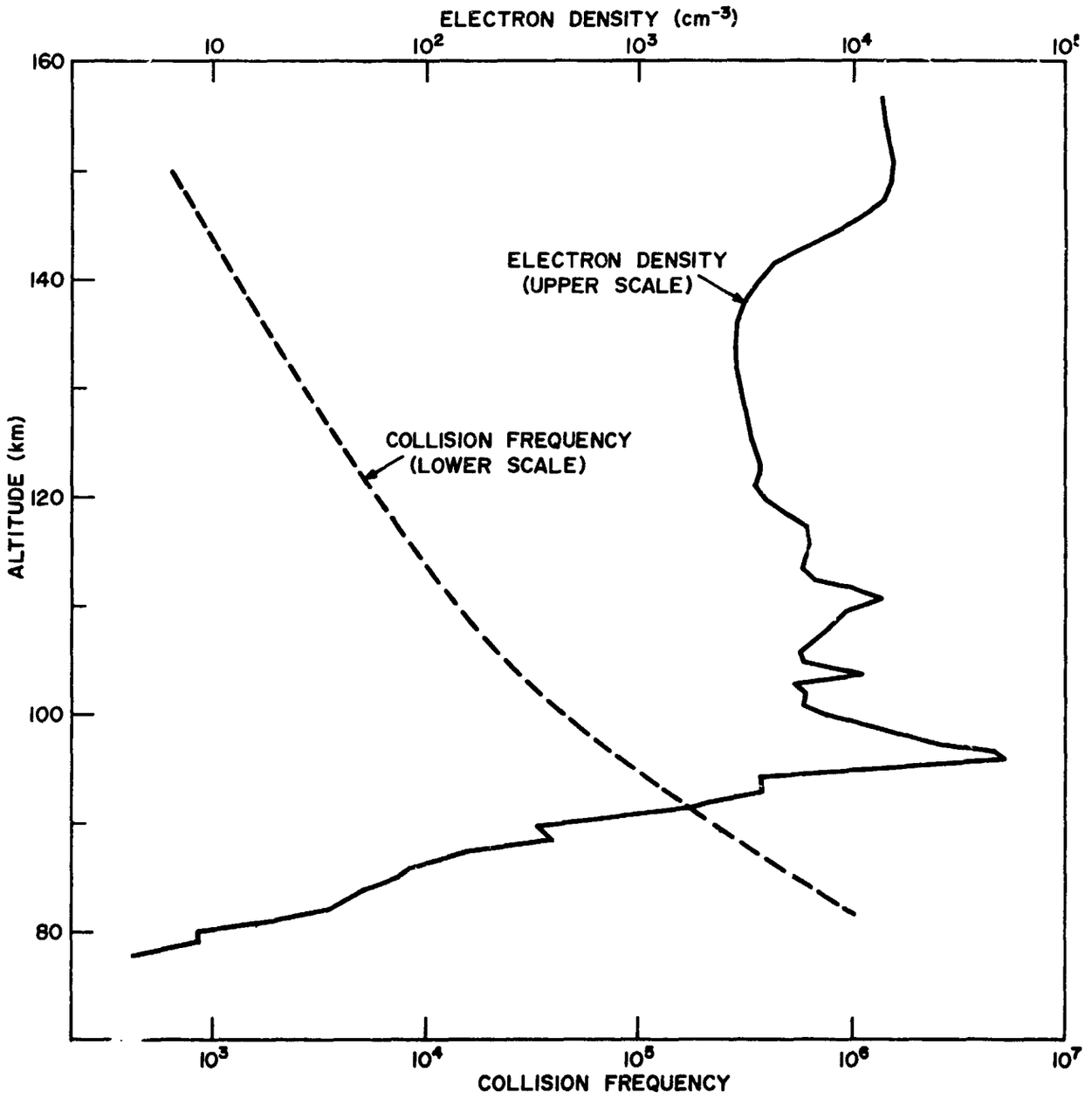

Figure 13 Electron density measured by Smith and Bedinger (1965) from their Fl. 14.194 flown at 1023 u.t. on October 8, 1964 from Wallops Island, Virginia and nighttime electron-neutral collision frequency computed by Brown (1962).

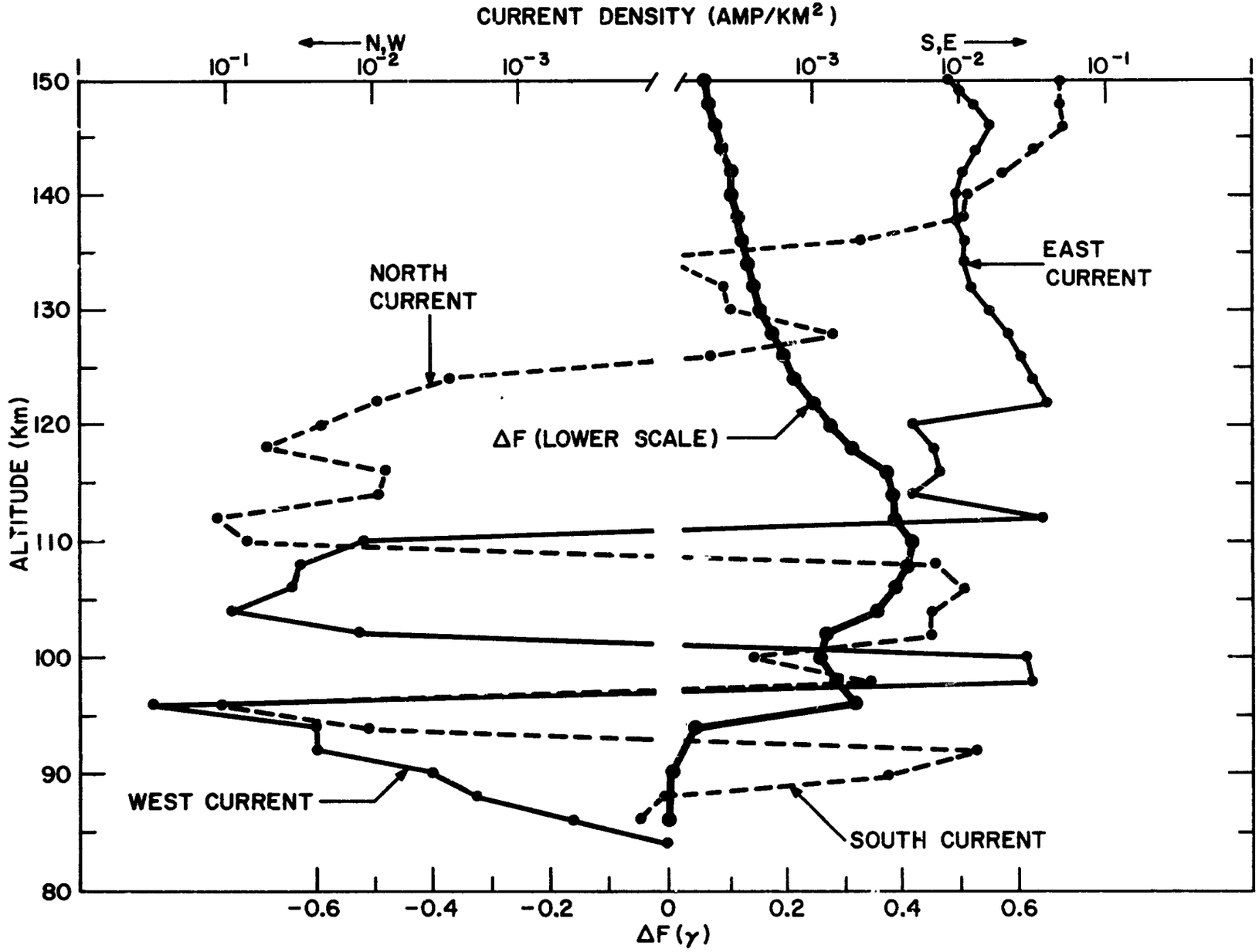

Figure 14 Calculated current densities at the time of Fl. 14.159 (10^h on October 8, 1964) and the resulting change in scalar magnetic field (ΔF) referenced to the bottom edge of the current layer.